Mon. Not. R. Astron. Soc. **000**, 000–000 (0000) Printed 23 October 2014 (MN LATEX style file v2.2)

The dynamics of collapsing cores and star formation

Eric Keto[1⋆], Paola Caselli[2], Jonathan Rawlings[3]
[1] *Harvard-Smithsonian Center for Astrophysics, 160 Garden St, Cambridge, MA 02420, USA*
[2] *Max Planck Institute for Extraterrestrial Physics, Glessenbachstr. 1, D-85741, Garching, Germany*
[3] *University College London, Gower St, London WC1E 6BT, United Kingdom*

arXiv:1410.5889v1 [astro-ph.SR] 22 Oct 2014

October 21, 2014

ABSTRACT

Low-mass stars are generally understood to form by the gravitational collapse of the dense molecular clouds known as starless cores. Continuum observations have not been able to distinguish among the several different hypotheses that describe the collapse because the predicted density distributions are the almost the same, as they are for all spherical self-gravitating clouds. However, the predicted contraction velocities are different enough that the models can be discriminated by comparing the velocities at large and small radii. This can be done by observing at least two different molecular line transitions that are excited at different densities. For example, the spectral lines of the H_2O $(1_{10} - 1_{01})$ and $C^{18}O$ $(1 - 0)$ have critical densities for collisional de-excitation that differ by 5 orders of magnitude. We compare observations of these lines from the contracting starless core L1544 against the spectra predicted for several different hypothetical models of contraction including the Larson-Penston flow, the inside-out collapse of the singular isothermal sphere, the quasi-equilibrium contraction of an unstable Bonnor-Ebert sphere, and the non-equilibrium collapse of an over-dense Bonnor-Ebert sphere. Only the model of the unstable quasi-equilibrium Bonnor-Ebert sphere is able to produce the observed shapes of both spectral lines. This model allows us to interpret other observations of molecular lines in L1544 to find that the inward velocities seen in observations of $CS(2 - 1)$ and N_2H^+ are located within the starless core itself, in particular in the region where the density profile follows an inverse square law. If these conclusions were to hold in the analysis of other starless cores, this would imply that the formation of hydrostatic clouds within the turbulent interstellar medium is not only possible but not exceptional and may be an evolutionary phase in low-mass star formation.

1 INTRODUCTION

The hypothesis that starless cores are the future birthplaces of low mass stars (Myers 1983; Myers & Benson 1983; Beichman et al. 1986) has proven an enduring point amidst continuing revision in the theories of how these cores actually evolve toward star formation. For example, one of the earlier suggestions that the gravitational collapse of star-forming clouds such as the starless cores occurs via a Larson-Penston (LP) flow (Larson 1969; Penston 1969), was later criticized (e.g. Shu 1977) because of its very particular initial conditions. In the LP solution, an initial velocity of 3.3 times the sound speed is required to pass a critical point in the flow. Shu (1977) proposed an alternative initial state, the singular isothermal sphere (SIS), leading to a different evolution described as "inside-out" collapse. This hypothesis was in turn criticized on similar grounds, namely that the (SIS) is unrealizable as an initial state owing to its dynamical instability (Whitworth et al. 1996). Alternatively it was proposed that the cores may be magnetically rather than hydrodynamically, supported against their self-gravity. Contraction then proceeds by ambipolar diffusion (Shu, Adams & Lizano 1987; Mouschovias 2001; Li 1999). This hypothesis faces challenges in that observations indicate that cores are supported predominantly by thermal pressure (Nakano 1998) and furthermore the magnetic diffusion time scale may be too slow (Tafalla et al. 1998; Ward-Thompson, Motte & Andre 1999). Another hypothesis suggests that the cores are hydrostatic or Bonnor-Ebert spheres (BES) partially supported by turbulent kinetic energy. Damping of this turbulent kinetic energy (Nakano 1998), which might be in equipartition with magnetic wave energy (Myers & Goodman 1988), allows the cores to contract in quasi-equilibrium (QE) (Keto & Caselli 2010; Broderick & Keto 2010). The model of the cores as BES has been criticized as incompatible with the larger-scale supersonic turbulence of the interstellar medium (ISM) (Ballesteros-Paredes, Klessen & Vázquez-Semadeni 2003). In this view, the turbulence creates transitory zones of compression where the distribution of dense gas merely resembles that in hydrostatic cores (Mac Low & Klessen 2004).

The scientific debate continues. Foster & Chevalier (1993) have suggested that an LP flow can develop in the contraction of a sphere whose initial state is both out of equilibrium and gravitationally unstable. Ciolek & Basu (2000)

© 0000 RAS

suggest how to reconcile the hypothesis of ambipolar diffusion with observations. The BES description, enhanced to include non-isothermal gas (Evans et al. 2001) chemical abundance variations (Keto & Caselli 2008), and perturbative oscillations (sonic waves) (Keto et al. 2006; Broderick & Keto 2010), continues to prove both descriptive and predictive of a wide range of observations (Alves, Lada & Lada 2001; Tafalla et al. 2002; Lada et al. 2003; Caselli et al. 2010, 2012; Nielbock et al. 2012).

One difficulty in discriminating among these hypotheses for contraction toward star formation is that some of the observed properties of the cores can be explained by more than one theoretical model. For example, self-gravitating spherical clouds develop a density profile scaling as the inverse square of the radius under a wide range of conditions. Figure 1 shows the gas densities in the three different evolutionary models with spherical symmetry, the LP flow, the inside-out collapse of the SIS, and the contraction of a QE-BES. The different density profiles are close enough to a $1/r^2$ profile to be observationally indistinguishable. The non-spherical models, ambipolar diffusion and large-scale turbulence can also produce similar density profiles (Ballesteros-Paredes, Klessen & Vázquez-Semadeni 2003; Ciolek & Basu 2000) but a detailed comparison with these more complex models is beyond the scope of this paper.

Although the density profiles are similar in all self-gravitating spherical clouds regardless of the mode of contraction, the internal velocities are quite different. Figure 2 shows that the velocities in the LP, SIS, and QE-BES models are sufficiently different that the underlying model can be deduced from the observations simply by comparing velocities at large and small radii. While the velocities in the spherical hydrodynamic models are quite specific, it is difficult to specify velocities for the hypotheses of turbulent compression or ambipolar diffusion. In the former case, the velocity profiles can be quite varied (Ballesteros-Paredes, Klessen & Vázquez-Semadeni 2003) because of the random nature of turbulence. In the latter case, the number of free or unconstrained parameters including the geometry of the magnetic field and the spatial distribution of magnetic field strengths allows for diverse outcomes (Li 1999; Ciolek & Basu 2000). In this paper we will set aside these last two hypotheses to await more statistical tests and focus on discriminating among the velocity profiles of the more uniquely defined spherical models.

Because of the approximate $1/r^2$ relationship between density and radius in all three spherical models, it is possible to measure the contraction velocity at small and large radii by observing spectral lines from molecules that are excited or abundant at different densities. We have observations of two such molecular lines for the contracting core L1544. Owing to its large Einstein A coefficient (3.5×10^{-3} s^{-1}), the 556.936 GHz emission line of H_2O ($1_{10} - 1_{01}$) serves as a tracer of dense gas ($\gtrsim 10^6$ cm^{-3}) that isolates the conditions in the very center ($r < 0.01$ pc) of the core (Keto, Rawlings & Caselli 2014). In contrast, the 109.782 GHz $C^{18}O$ (1-0) transition has a critical density that is 5 orders of magnitude smaller. Thus the observed $C^{18}O$ line is dominated by the emission from the outer regions of the cloud where there is more volume and more column density.

In this paper, we compare observations of these two spectral lines from the contracting core L1544 against the line spectra predicted for 5 different spherical models as follows:

(i) The contraction of a quasi-equilibrium Bonnor-Ebert sphere (QE-BES) (Keto & Caselli 2010).

(ii) The contraction of a non-equilibrium Bonnor-Ebert sphere (NE-BES) (Foster & Chevalier 1993).

(iii) A static sphere.

(iv) The Larson-Penston (LP) flow (Larson 1969; Penston 1969).

(v) The inside-out collapse of the singular isothermal sphere (SIS) (Shu 1977).

Since a BES is in hydrostatic equilibrium by definition, the terminology of a quasi-equilibrium BES or non-equilibrium BES sounds self-contradictory and requires some explanation. Both the QE-BES and NE-BES are approximate BES related to a true BES by construction. The QE-BES is constructed as an unstable BES and allowed to evolve hydrodynamically. In the early stages, the QE-BES resembles a BES except in the center which evolves out of equilibrium most rapidly (figure 3). The NE-BES is constructed from an unstable or nearly unstable BES that is given a 10% increase in density everywhere and allowed to evolve. Because it is out of equilibrium everywhere, the contraction of NE-BES proceeds differently from a QE-BES. It begins collapse on all scales at once (figure 3).

Our investigation finds that the contracting QE-BES model provides a reasonable match to the observed emission lines H_2O ($1_{10} - 1_{01}$) and $C^{18}O$ (1-0) of the starless core L1544. The comparison with the other models indicates how close the contraction in L1544 is to quasi-equilibrium. For example, the QE-BES, the NE-BES, and the SIS all have an inside-out type of contraction with higher velocities toward the center, but with observable differences. For example, the NE-BES produces a $C^{18}O$ spectral line profile that does not fit the observed $C^{18}O$ line because its overall contraction has higher velocities in the outer core that split the predicted $C^{18}O$ line in a way that is not observed. The SIS with its continuously increasing velocities at smaller radii predicts an H_2O line with a larger split than observed.

In this paper we also use the conceptual framework of the QE-BES model to interpret other observations in the literature bearing on the evolution of the starless cores towards star formation. In particular, we model the CS(2-1) and N_2H^+(1-0) emission in L1544 to precisely locate the "extended inward motions" (Tafalla et al. 1998; Myers, Evans & Ohashi 2000) in starless cores. We find that the N_2H^+ emission comes from the central 5000 au (half-width radius at half-maximum (HWHM)) where the gas density is $\gtrsim 10^5$ cm^{-3}. The CS(2-1) emission comes from within 10,000 au (HWHM) which is within the $1/r^2$ region of the QE-BES density profile. In particular, we find that the comparison of the CS and N_2H^+ lines does not support an interpretation of inward flow from scales larger than the starless core.

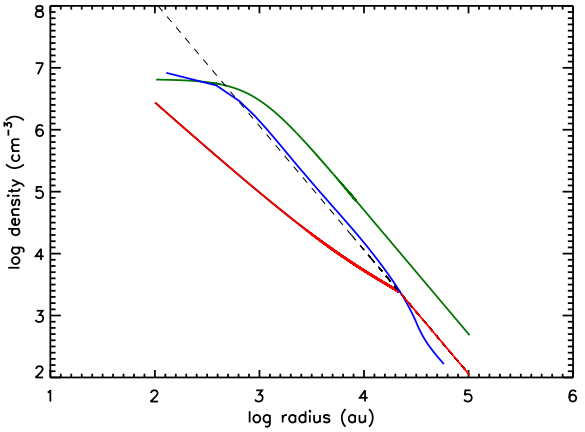


Figure 1. Densities (*right*) in 3 models of spherical contraction. The green line (upper) shows the Larson-Penston flow. The red line (lower) shows the inside-out collapse of a singular isothermal sphere. The blue line (middle) shows the quasi-equilibrium contraction of an unstable Bonnor-Ebert sphere. The dashed line shows a r^{-2} profile for reference.

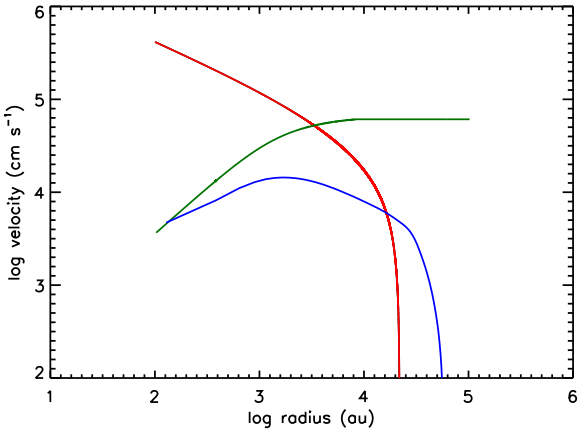


Figure 2. Velocities in the same 3 models of spherical contraction as in figure 1. In contrast to the density profiles, the velocity profiles of these 3 models are sufficiently different to be observationally distinguishable. The green line (middle) shows the Larson-Penston flow, the red line (upper) shows the inside-out collapse of a singular isothermal sphere, and the blue line (lower) shows the quasi-equilibrium contraction of an unstable Bonnor-Ebert sphere.

2 DATA

The H_2O and CO spectra are the same data as used in Keto & Caselli (2010) and Keto, Rawlings & Caselli (2014). The water line was observed with the Herschel Space Observatory and originally reported in Caselli et al. (2012). The $C^{18}O$ line was observed with the IRAM 30m and originally reported in Caselli et al. (1999).

Observations of the CS(2-1) line are reported in the literature (Tafalla et al. 1998; Myers, Evans & Ohashi 2000; Lee, Myers & Tafalla 2001) and provide further information on the nature of the contraction. This transition has a critical density of 6×10^5 cm^{-3} intermediate between H_2O and $C^{18}O$. Unlike the $C^{18}O$, the CS transition is optically thick in L1544. Differential self-absorption of the line emission in a velocity gradient makes this transition a sensitive indicator of velocity. We refer to the CS(2-1) spectra in the literature in a qualitative comparison with the predicted spectra.

3 THE DYNAMICAL MODELS

Our BES models which include the QE-BES, NE-BES and the static BES are calculated with the 1D Lagrangian numerical hydrodynamic code described in Keto & Field (2005). This code includes radiative heating and cooling of the gas and dust and simplified CO and H_2O chemistry to set the abundances of the major gas coolants (Keto, Rawlings & Caselli 2014). These abundances are also used in the radiative transfer calculations that simulate the observed spectral lines.

The QE-BES model starts with a central density of 10^4 cm^{-3}, and the Lane-Emden density profile is truncated – the external pressure is set equal to the internal pressure at the boundary – at a radius that gives the cloud a mass of 10 $M_\odot$. This is the same model used in our earlier research (Keto & Caselli 2008, 2010). The modeled mass is approximately the same as the 8 $M_\odot$ estimated from CO observations of L1544 itself, excluding the L1544-E and L1544-W companions (Tafalla et al. 1998). The initial density at the start of the hydrodynamic evolution cannot be known from observations. Ours is chosen to be high enough that the core is gravitationally unstable and low enough that the core has time to evolve before reaching the observed central density of about 10^7 cm^{-3}. This density was deduced earlier (Keto & Caselli 2010) by comparison of the observed and predicted CO and N_2H^+ spectra.

The initial state is one of gravitationally unstable hydrostatic equilibrium. Any perturbation of this structure will result in collapse. Even a slight *decrease* in the overall density will cause the core to contract because there is no adjustment that leads to stable equilibrium. The collapse progresses from the inside-out with the center moving out of equilibrium soonest and fastest. The progression of velocities and densities during the evolution is shown in figure 3. We call this mode of contraction quasi-equilibrium (QE) because wherever the contraction velocities are subsonic, the density structure resembles a static equilibrium core. This is characteristic of an unstable BES during the sonic phase of contraction (Larson 1969; Foster & Chevalier 1993; Ogino, Tomisaka & Nakamura 1999; Keto & Caselli 2010).

We construct an NE-BES by finding the equilibrium BES for a 9.1 $M_\odot$ core with the same central density of 10^4 cm^{-3} as the QE-BES. We then increase the density everywhere by 10% similar to the procedure in Foster & Chevalier (1993) so that the core now has 10 $M_\odot$ but with the density profile appropriate for a 9.1 $M_\odot$ core. This initial state is also gravitationally unstable, but nowhere in equilibrium. As a result, this core begins to contract immediately and everywhere at once. Figure 3 compares the densities and velocities of the the QE-BES and NE-BES models during the evolution. The most significant difference is in the velocities at large radii. To compare with the observations we use the model at the evolutionary time when the central density is 10^7 cm^{-3}, same as the model of the QE-BES.

Our third model, the static core, is calculated as a 10

$M_\odot$ BES with a central density of 10^7 cm^{-3}. The density structure of this core is quite similar to the QE-BES and the NE-BES with the same central densities (figure 3).

The LP and SIS models are calculated by integrating equations 11 and 12 in Shu (1977). The sound speed for both models is 0.2 kms^{-1} ($\sim$ 11 K), and the evolutionary times are 2.8×10^{11} and 8×10^{12} seconds respectively, chosen so that the density profiles are qualitatively close to that of the contracting BES model (figure 1).

The predicted spectral lines for all five models are calculated with our radiative transfer code MOLLIE (Keto 1990; Keto & Rybicki 2010) which also computes the chemical abundances (Keto & Caselli 2008; Keto, Rawlings & Caselli 2014) for the LP and SIS models.

The LP and SIS models are isothermal in contrast to our BES models and in contrast to the observations (Crapsi et al. 2007) that also indicate a range in temperature from 6 - 18 K in L1544. This discrepancy is not a concern for this study. First, this range in temperature has little effect on the dynamics (Keto & Caselli 2010). Second, in this study we use the line profiles in our model-data comparisons, particularly the splitting of the spectral lines by the velocities, rather than the absolute brightness of the lines. The former is a function of the gas velocities and the latter of gas temperature. The correlation between the velocity and gas temperature (colder in the center) affects the spectral line profile, but we will see in section §5 that this is not a problem for this conclusions of the comparisons.

4 THE MODEL FOR THE MOLECULAR ABUNDANCES

We use simplified models for the gas phase abundances of CO and H_2O following our earlier research (Keto & Caselli 2008; Keto, Rawlings & Caselli 2014). Figure 4 shows the abundances as a function of radius along with the density, temperature, and velocity of the QE-BES at the evolutionary time when the central density reaches 10^7 cm^{-3}. Both the CO and H_2O are depleted from the gas phase at high densities ($\gtrsim 10^5$ cm^{-3}) where the molecules are frozen onto dust grains. In contrast, the abundance of N_2H^+ is assumed to remain volatile at all densities across the core.

Despite the gas phase depletion at high density, we know that that the H_2O ($1_{10} - 1_{01}$) line emission comes from the very center of L1544. The critical density for collisional de-excitation of this transition is 10^8 cm^{-3} assuming 10 K and para-H_2 (Dubernet et al. 2009; Keto, Rawlings & Caselli 2014). The maximum gas density, 10^7 cm^{-3}, in our model of L1544 never reaches this critical density and the transition is sub-critically excited (Keto, Rawlings & Caselli 2014). The volume of gas with high density, for example above 10^6 cm^{-3}, is quite small (radii $<$ 0.005 pc) and the H_2O abundance is very low ($< 10^{-12}$ relative to H_2). The combination of a low column density and sub-critical excitation means that the H_2O ($1_{10} - 1_{01}$) emission is very weak (0.025 K), but serves the purpose of reporting on the conditions in the core center.

In contrast, the critical density for the $C^{18}O$ (1-0) transition (2×10^3 cm^{-3}) is 5 orders of magnitude smaller than for our H_2O transition. The volume of gas in L1544 with a density high enough to excite $C^{18}O$ is much larger (within 0.14 pc) than the volume able to excite H_2O. Accordingly, the $C^{18}O$ (1-0) line emission is much brighter (5 K) than the H_2O line. While there is still $C^{18}O$ emission from the center of the core, its contribution to $C^{18}O$ line emission is insignificant. The $C^{18}O$ line is dominated by the large volume and high column density gas in the outer cloud.

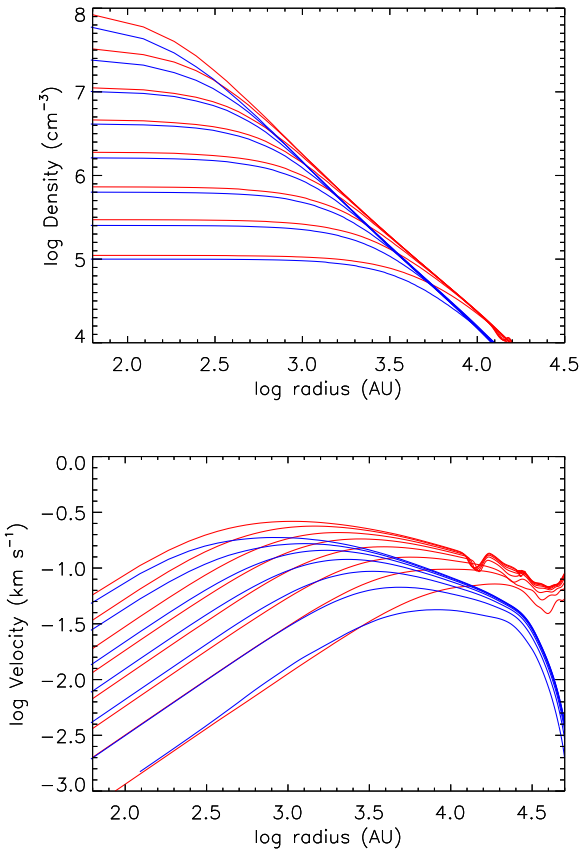


Figure 3. Comparison of densities (*top*) and velocities (*bottom*) in quasi-equilibrium (QE) (*blue*) and non-equilibrium (NE) (*red*) contraction at different evolutionary times. The calculation shows increasing densities and velocities, upward in both figures as the contraction progresses. The density structure in both modes of contraction continues to resemble a static BES whose central density is increasing with time. The velocities are also nearly the same in the center of the core resulting in nearly identical H_2O spectra. However, the velocities are quite different in the outer core, tending to zero in the quasi-equilibrium case and remaining nearly constant with both time and radius in the non-equilibrium case. This difference is noticeable in the predicted CO spectra labeled QE-BES and NE-BES in figure 5.

5 COMPARISON AND INTERPRETATION

5.1 The QE-BES

The predicted spectra for the contraction of the QE-BES are shown in figure 5 and compared with the observed spectra. The H_2O spectrum shows an inverse P-Cygni type profile with red and blue shifted absorption and emission, respectively, consistent with the inward velocities of contraction. Since this emission must come from the highest density gas,

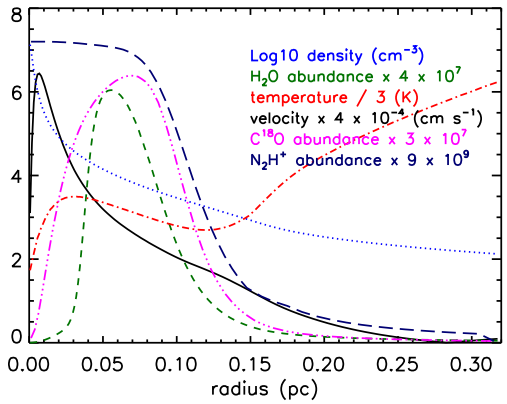


Figure 4. Physical conditions in the QE-BES model for L1544. The vertical axis has different units depending on the quantity displayed. The solid black line shows the velocity in cms $^{-1}$ multiplied by 4×10^{-4}. The dotted blue line shows the log of the density (cm^{-3}). The red dot-dash line with 1 dot shows the temperature in K divided by 3. The green dashed line shows the abundance of H_2O relative to H_2 multiplied by 4×10^7. The purple dot-dash line with 3 dots shows the abundance of $C^{18}O$ relative to H_2 multiplied by 3×10^7. The blue line with large dashes is the abundance of N_2H^+ multiplied by 10^{10}. The other models, NE-BES, static BES, LP, and SIS, have similar temperatures, densities, and abundances, but different velocities.

these velocities are in the core center. In contrast, the CO line, whose emission is dominated by the greater volume of gas at larger radii, is completely unaffected by the high velocities in the center of the core that split the H_2O line. As a result, the CO line is only slightly broadened, and this is caused entirely by the low velocities in the outer part of the QE-BES.

In the H_2O spectrum, the absorbed background is the submillimeter dust continuum, and this has been subtracted from both the predicted and observed spectra. At the frequency of the CO line the dust continuum is negligible so there is no absorption.

The evolutionary time of the contraction is of course not known, and we choose a time in the modeled contraction to match the observations. In our earlier paper (Keto & Caselli 2010) we chose the point in the evolution when the central density reaches 10^7 cm^{-3} based on comparison with CO and N_2H^+ spectra. The observed H_2O ($1_{10} - 1_{01}$) line provides additional constraint. Models with much lower central density will not excite the H_2O transition enough to match the observation. The observed line profiles and widths constrain the model to evolutionary stages before the development of supersonic velocities in the emitting regions. The maximum velocity (0.15 kms^{-1}) in our selected model is just below the sound speed (0.2 at 10 K).

5.2 The NE-BES

The predicted spectra for the contraction of the non-equilibrium sphere are shown in figure 5. This model is qualitatively similar to one studied in Foster & Chevalier (1993) except that our model is not isothermal and therefore not scale-free. However, as noted in Keto & Caselli (2010) this has a negligible effect on the dynamics. The predicted H_2O emission is slightly broader than in the spectrum from the QE-BES but negligibly different given the noise in the observed spectrum. The predicted CO spectrum is quite different, noticeably split by the higher velocities in the outer region of the NE-BES. Our predicted CO spectrum is essentially the same as the generic optically thin spectrum predicted in Foster & Chevalier (1993) and shown in their figure 6. The only difference is that ours shows a slight blue-dominated asymmetry consistent with spherical contraction. This asymmetry from self-absorption is not expected in the optically thin approximation of the radiative transfer used in Foster & Chevalier (1993).

5.3 The static BES

As a point of reference, the spectra predicted for the model of a static BES are shown in figure 5. In this case, the cold H_2O outside the core center absorbs not only the dust continuum but also all the H_2O emission. The CO line is narrower than for either of the contracting models, and a little brighter since all the emission is concentrated in a smaller width.

5.4 The LP flow

The spectra predicted for the LP flow are compared with the observed spectra in figure 5. In the LP solution there are two scaling parameters, the sound speed and the evolutionary time that affect the densities and velocities. We use a sound speed of 0.2 kms^{-1}, the same as in Shu (1977) and consistent with our non-isothermal models. The evolutionary time is more arbitrary. We have chosen a time (2.8×10^{11} s) to best match the observed H_2O and $C^{18}O$ spectra. However, even the best correspondence is not good because of the supersonic velocities in this model. While the LP flow is a very specific model, the comparison suggests that any model of contraction that has a high velocity inflow in the outer part of the core is going to have trouble matching the CO spectrum regardless of the details of the model.

5.5 The SIS

The spectra predicted for the inside-out collapse of the SIS are compared with the observed spectra in figure 5. Both the H_2O and CO spectra show that the velocity profile is not quite correct. This is not easy to fix. The velocity profile depends on the evolutionary time, 8×10^{12} s in our model. At earlier evolutionary times, the velocity profile has a narrower range of velocities on the relevant core radii (> 100 au). However, this also narrows the absorption feature in the H_2O spectrum and allows the redshifted emission feature to become as bright as the blue feature. On the other hand, at later evolutionary times, the increased range of velocities increases the width of the CO line.

One of the notable characteristics of the observed spectral line profiles in many Taurus cores is the lack of high velocity wings. The lack of high velocities is a critical feature that identifies the starless cores among the other clouds in the supersonic turbulent ISM. The high velocities in the SIS model are problematic in this regard.

Another difficulty with the SIS model is the sensitivity

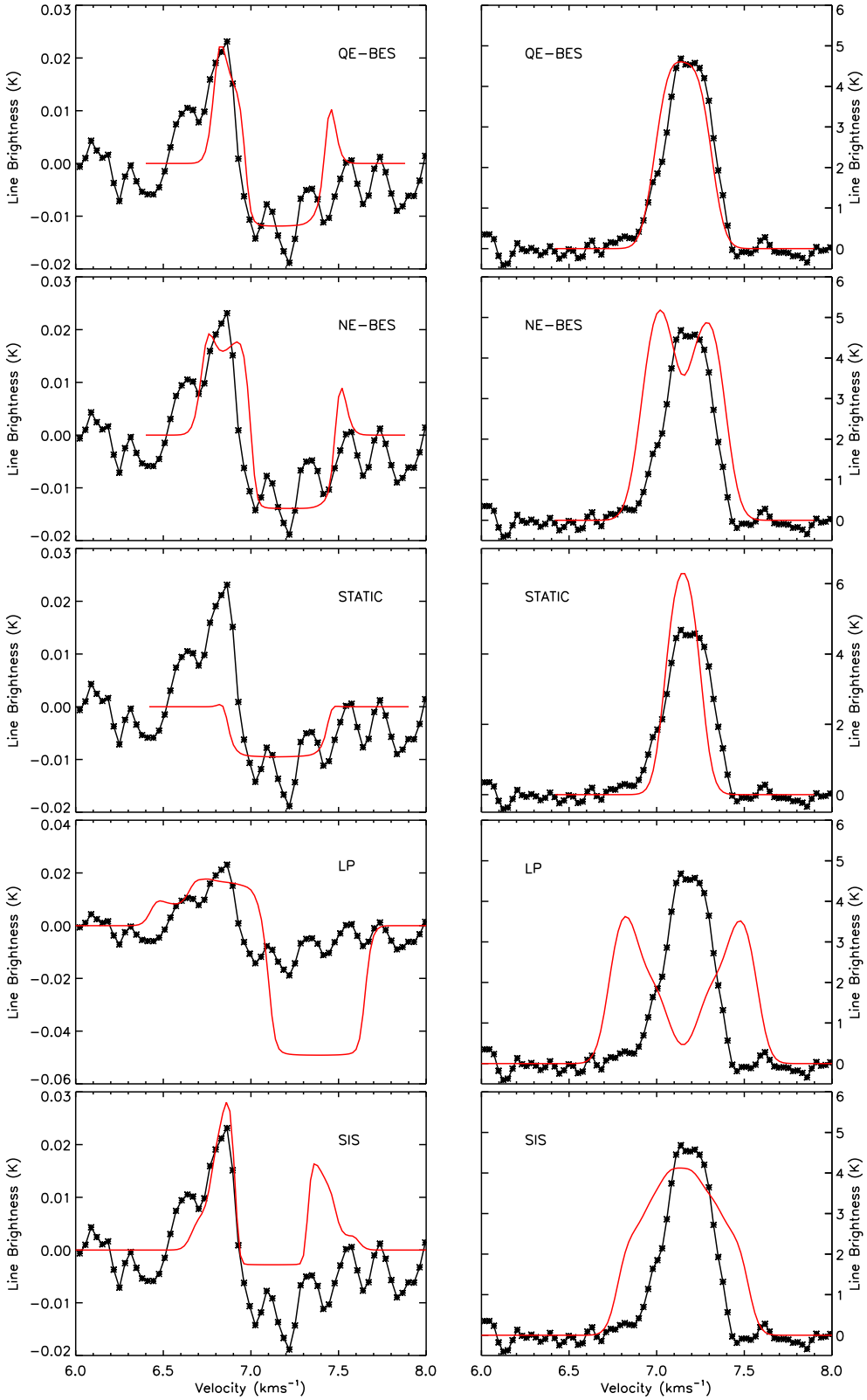


Figure 5. Observed spectra (black line with symbols) compared with spectra predicted (plain red line) for the five models of starless cores. The left and right columns show the H_2O and $C^{18}O$ spectra, respectively. The five models from top to bottom are: 1) an unstable Bonnor-Ebert sphere in quasi-equlibrium contraction (QE-BES), 2) a Bonnor-Ebert sphere with a 10% over density in non-equilibrium collapse (NE-BES), 3) a static Bonnor-Ebert sphere (static), 4) a Larson-Penston flow (LP), and 5) a singular isothermal sphere (SIS) in inside-out collapse. Owing to their different critical densities for collisional de-excitation, the H_2O and $C^{18}O$ lines are generated in the inner and outer regions of the core, respectively. Only the QE-BES model has the correct contraction velocities in both regions to produce spectral line profiles matching both observations.

of the width of the predicted line profiles to the evolutionary time which is the parameter that scales the range of inward velocities. A group of SIS cores at different evolutionary times would have individual cores with different maximum velocities and therefore different line widths. This is not indicated by the observations. Among the many spectral line observations of cores in the literature, we do not find a range of line widths or profiles from subsonic to supersonic as would be observed in SIS cores at different evolutionary times.

In contrast, the QE-BES does not have this sensitivity to evolutionary time. Once the central density of a quasi-equilibrium contracting BES reaches a certain density ($\sim 10^5 - 10^6$ cm^{-3}) the predicted line profiles, taking account of the angular resolution of the single-dish beams, do not change much as the core evolves until the velocities become supersonic in the inner core over a region comparable to the single dish beam size ($\sim$ 1000 au).

6 EXTENDED INWARD MOTIONS IN THE QE-BES

There are two other observations in the literature whose interpretation we wish to address in the context of the QE-BES model. First, observations of CS(2-1) show spectra asymmetrically split by self-absorption in a line profile characteristic of inward motion (figure 7 of Tafalla et al. 1998). The splitting is seen in spectra taken at positions out to a projected radius of about 16000 au, assuming a distance to L1544 of 140 pc. This pattern is also seen in other cores in the Taurus star forming region (Lee, Myers & Tafalla 2001). As suggested in the references above, the comparison of the observed CS and N_2H^+ lines indicates inward flow from an extended region defined by the CS emission onto a smaller region of dense gas defined by the extent of N_2H^+ emission. With the model of the QE-BES, we can interpret these observations more precisely.

Figure 2 shows that the QE-BES model for L1544 has inward velocities out beyond 16000 au or 100 arc seconds, again assuming a distance of 140 pc. While these extended inflow velocities only slightly broaden the optically thin $C^{18}O$ line (figure 5) they cause asymmetric self-absorption in optically thick lines such as CS(2-1). The simulated CS(2-1) spectra show split asymmetric spectra extending almost to the boundary of the core. Figure 6 shows these spectra to 16000 au where the lines become so weak that observational noise would hide the splitting. A comparison with figure 3 shows that these spectra are generated within the $1/r^2$ region of the QE-BES.

The difference between the spatial extents of the CS and N_2H^+ emission and the difference in their spectral line profiles are easily understood as arising from their respective abundances and variations in abundance with density. The CS molecule is about 100 times as abundant as N_2H^+ (van Dishoeck & Blake 1998; Keto & Caselli 2010). Since both molecules have similar Einstein A coefficients and similar critical densities for collisional de-excitation, the greater abundance of CS makes this molecule brighter than N_2H^+ in lower density gas.

Based on our earlier research (Keto & Caselli 2010), we assume that all the N_2H^+ remains in the gas phase across the core. For our purposes, this is consistent with Caselli et al. (2002) who found that N_2H^+ was depleted by a factor of 3 in the center of L1544. This is much smaller than the depletion of CO which is almost complete at the highest densities in L1544.

Our simple chemical models do not include sulfur species. In the cold cores, the dominant processes controlling the abundance are photo-dissociation and freeze-out which we assume to be similar for CS and CO. We know that there are differences in the gas phase chemistry of CS and CO particularly at high densities, but because the gas phase abundance of both molecules is decreasing rapidly by freeze-out at these same densities, the spectral lines of both molecules are dominated by the emission from the outer core where the abundances are similar. However, the maximum brightness in our CS line is just under 5 K, a little brighter than the peak brightness in the observed line, just under 4 K.

If we assume that most of the CO in L1544 is in $C^{16}O$, and we adopt the $C^{16}O/C^{18}O$ ratio of 560 suggested by Wilson & Rood (1994), this fixes the total carbon abundance relative to H_2 at 1.3×10^{-4} and the maximum CS abundance (neither depleted nor photo-dissociated) at 3×10^{-8} relative to H_2. However, because the CS line is optically thick, the intensity is not very sensitive to the abundance.

Figure 7 shows the spatial variation of the peak brightness of CS(2-1) and N_2H^+(1-0) in the QE-BES model as calculated by our radiative transfer simulation. The simulation shows that in the QE-BES model, the extent of the CS emission is twice that of the N_2H^+. The spatial half width at half maximum (HWHM) of the simulated peak emission of the CS(2-1) is 8200 au or 0.04 pc. This may be compared to the observed HWHM of 10300 au or 0.05 pc (Lee, Myers & Tafalla 2001). The width in the CS simulation includes convolution with a 48" FWHM beam to match the beam of the observations. The spatial HWHM of the modeled N_2H^+ emission is 5100 au or 0.025 pc. This may be compared to an observed HWHM for the N_2H^+ emission of 5000 au or 0.025 pc (Lee, Myers & Tafalla 2001) and 6000 au or 0.03 pc (Caselli et al. 2002). The difference in the extent of the CS emission between the model and the observations may be due to the approximation of spherical symmetry in the model whereas L1544 is observed to have an axial ratio of 2:1. The observationally determined radius includes this spatial asymmetry since it is measured as $\sqrt{A/\pi}$ where A is the area of the cloud within the HWHM contour. Our approximate treatment of the CS abundance may also contribute to this discrepancy.

Since N_2H^+ has a nearly constant abundance (we assume 3×10^{-10}) inside the photo-dissociation boundary, its line brightness scales with the column density. However, owing to its low abundance, the N_2H^+ line is optically thin except in the very center of the core where the hyperfine lines are seen to be just barely split by self-absorption(figure 9 of Keto & Caselli 2010). The smaller splitting does not indicate lower velocities in the inner core than in the outer, just lower optical depth of the molecular tracer. In general the magnitude of the inward velocities cannot be inferred only from the width of the splitting due to self-absorption. The observed separation of the split peaks is due to a combination of the velocity and the optical depth so the strength of the self-absorption must be known as well.

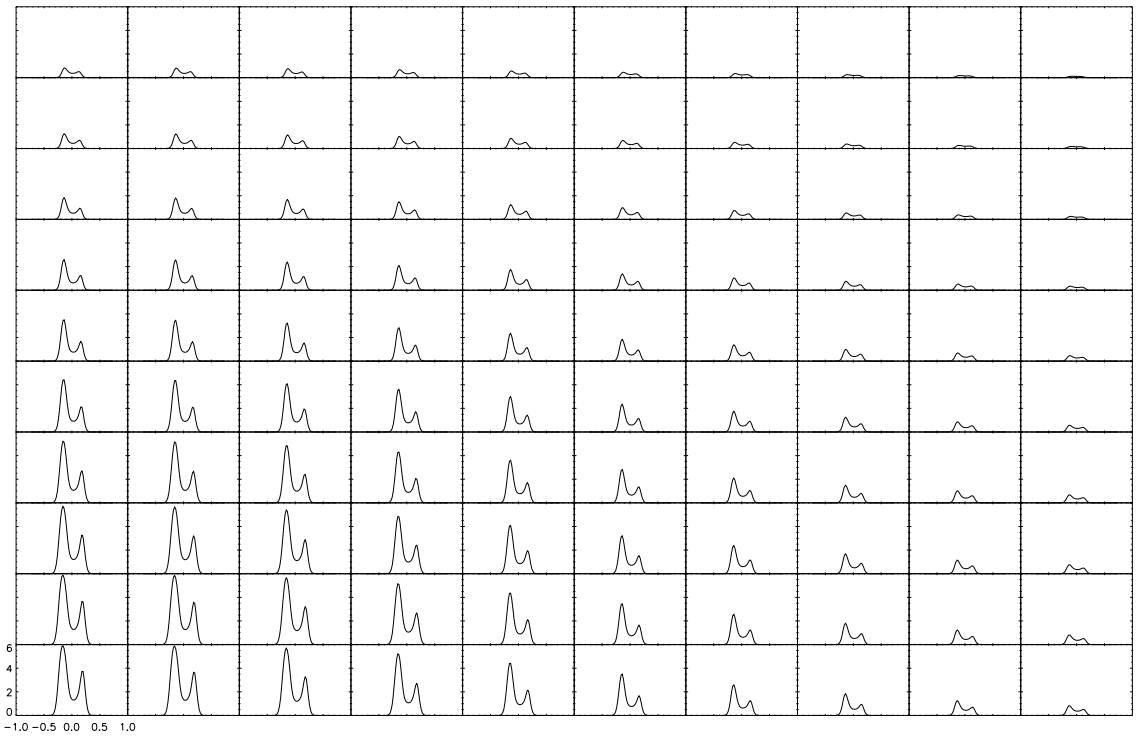


Figure 6. Map of CS(2-1) emission predicted from the model of the BES contracting in quasi-equilibrium. The center of the model is the lower left corner. The map shows 1/4 of the spherical model. The velocity axis ranges from -1 to +1 in the rest frame of the cloud. The brightness ranges from 0 to 5 K. The spacing of the spectra is 2000 au showing that the infall asymmetry is evident out to a radius of 16000 au.

It is correct to infer that the bright N_2H^+ emission arises from the densest part of the core and that there is contraction from the outer core onto this dense region. However, the observations of the H_2O line indicate even higher contraction velocities in the dense inner core. Furthermore, the CS and N_2H^+ spectra do not indicate inward velocities extended beyond the core. The inward velocities responsible for splitting the CS spectra are entirely within the core.

Another simple line of reasoning leads to a similar conclusion. We know that L1544 is bounded by a photo-dissociation region that is necessarily created by the external UV radiation that is required to produce the outwardly increasing gas temperature (Evans et al. 2001; Crapsi et al. 2007) and the gas phase abundance of H_2O resulting from photo-desorption (Keto, Rawlings & Caselli 2014). Setting aside the complex radiative transfer arguments, we know that the molecular line emission must come from the molecular side, the inside, of the photo-dissociation boundary.

Alternatively, the outer boundary can also be defined observationally as a transition to coherence (Goodman et al. 1998; Pineda et al. 2010). The observed width and splitting of the CS line indicates subsonic velocities. This places the CS emission within (on the subsonic side) of the transition to coherence. These considerations again place the extended inward motions within and not outside the QE-BES.

As correctly pointed out in Tafalla et al. (1998), inward velocities at the radii observed in L1544 are incompatible with the inside-out collapse of an SIS. In the SIS model, non-zero velocities at radii of 16000 au require an evolutionary time $\gtrsim 0.4$ Myr. This is the time required for the expansion wave initiating the infall to reach 15000 au. During this time, enough mass would have accreted into the center to form an easily detectable protostar (Tafalla et al. 1998). The QE-BES model does not have this inconsistency. In contrast to the SIS model, the central density in the QE-BES is only 10^7 cm^{-3} at the time that the inward flow extends beyond 30000 au (figure 1).

There is an interesting difference between the accretion rates of the SIS and QE-BES models. Whereas the accretion rate in the SIS is constant in time, the accretion rate in the QE-BES model is initially zero and increases with time. However, the characteristic time scale for collapse is essen-

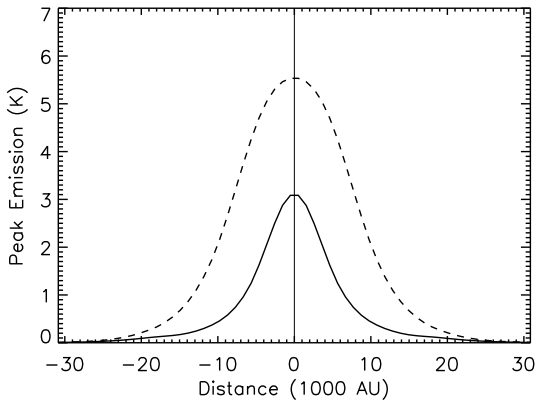


Figure 7. Comparison of the modeled spatial extent of the CS(2-1) (dashed lines) and N_2H^+(1-0) (solid line) emission across the L1544 core. The difference is mostly due to their different abundances. CS is about 100 times more abundant than N_2H^+.

tially the same in both models and is the free-fall or sound-crossing time. This comparison implies that in the QE-BES contraction, the formation and accretion onto a protostar occurs later than in the SIS, still within the collapse time of the entire core, but later within that time period.

7 SPECULATION ON THE ORIGIN OF THE QE-BES

Our study seeks to better understand how the clouds that we observationally identify as starless cores evolve toward star formation. The formation of the starless cores within the ISM is a topic for further research. However, we can speculate on the more general question of whether an unstable core such as the QE-BES is a suitable initial state for an evolutionary model. How is this unstable state created? Is this model subject to the same criticism as directed toward the SIS that this initial state is unrealizable because of its instability (Whitworth et al. 1996)? We imagine that an unstable BES may be created in a two step process. The first step is the creation of a stable BES out of the larger scale turbulent ISM and the second step is the evolution of the stable BES to instability. The second step is better understood and can be explained rather easily if we assume that stable cores can be created. We begin with the second step first.

7.1 The approach to instability

One process that leads a stable BES to instability, the dissipation of internal turbulent kinetic energy, was recognized immediately in the early observations that first identified the star-forming potential of the starless cores. "Observed distributions of dense core properties in Taurus, Ophiucus, and other dark cloud regions appear consistent with dense core evolution toward star formation via dissipation of turbulence (Myers 1983)". The internal subsonic turbulent kinetic energy is critical to the dynamical stability of the cores because thermal energy provides only a fraction of the internal energy needed to support a core against gravity and external pressure. For example, Myers & Benson (1983) suggested that the line widths of starless cores, equivalent to a 16 K Gaussian, show sufficient internal energy for virial equilibrium, but that the 10 K gas could account for only 60% of the kinetic energy indicated by the line width. The early observations also noted that star formation activity was associated with cores with less subsonic turbulence. From observations of 27 cores from Myers & Benson (1983) and 16 cores from Leung, Kutner & Mead (1982), Myers (1983) concluded "In complexes which are vigorously forming low-mass stars, dense cores are more prevalent, smaller, denser, and have narrower lines than in regions with less star formation. " These results were confirmed in a much larger survey of 179 cores by Tachihara et al. (2002) who noted smaller molecular line widths in star-forming cores than in starless cores. They also concluded that decay of the internal subsonic turbulence is necessary for star formation. More recently, a survey of cores in the Pipe nebula also shows many cores requiring turbulent energy in addition to thermal energy for equilibrium (Lada et al. 2008).

On the theoretical side, recent research (Keto et al. 2006; Broderick et al. 2007) identifies the complex spatial patterns of red and blue asymmetric self-absorbed spectral line profiles observed in some cores (Lada et al. 2003; Redman, Keto & Rawlings 2006; Aguti et al. 2007) as the long-wavelength modes of this turbulence or sonic oscillations in BES. On the basis of numerical simulations Broderick et al. (2007) concluded that long-wavelength oscillations, except for the (0,0,0) breathing mode, can indeed stabilize a BES. Analysis of wave transmission and reflection as a three-wave problem (Broderick et al. 2008) and non-linear mode-mode coupling by numerical simulations (Broderick & Keto 2010) indicates damping times for oscillations in BES of several 10^5 to just over 10^6 yr depending on the density contrast between the sphere and its surroundings.

The transition from a stable BES to an unstable QE-BES can be summarized as follows. For a given internal energy, including thermal and subsonic turbulence, expressible as an effective sound speed, and a given external pressure there is a maximum stable mass for a BES. As the turbulent energy dissipates, the critical mass lessens until it becomes equal to the actual mass. At this point the BES is at critical equilibrium and ready to begin its contraction as an unstable QE-BES with any subsequent loss of internal energy.

7.2 The formation of stable cores

On scales larger than the cores, the ISM is supersonically turbulent, yet the character of that turbulence is described differently in the literature. Numerical hydrodynamic simulations of the turbulent ISM generally suppose that the turbulence has an external driver that has produced the initial turbulent velocities and densities (Klessen et al. 2005; Offner et al. 2008). More conceptual models for the supersonic turbulence emphasize the dominance of internal gravitational rather than hydrodynamic forces in the supersonic turbulence of the ISM (Larson 1981; Field, Blackman & Keto 2011).

The numerical hydrodynamic simulations of the turbulent ISM have not yet produced stable cores. These results are interpreted differently. Klessen et al. (2005) and

Ballesteros-Paredes, Klessen & Vázquez-Semadeni (2003) suggest that the transient density fluctuations in their simulations of the turbulent ISM resemble BES and the interpretation of actual observations as indicating BES in the ISM is mistaken. However, Offner et al. (2008) interpret their own simulations otherwise: "The physical origin of the poor agreement between the simulations and observations appears to be that the simulated protostellar second-moment distributions ... do not have sufficiently narrow peaks. The protostellar cores in the simulations are at the centers of regions of supersonic infall, which contradicts the observations that show at most transonic contraction."

A discussion of the numerical hydrodynamical modeling of turbulence is beyond the scope of this paper other than to note the differences in opinion among numerical modelers. The very strong conclusion that "Reaching hydrostatic equilibrium in a turbulent molecular cloud environment is extremely difficult and requires strongly idealized conditions that are not met in the interstellar gas (Klessen et al. 2005)" is not shared by all researchers of the turbulent ISM. For example, the more conceptual model of the ISM turbulence of Field, Blackman & Keto (2011) suggests how the stable starless cores might be created.

Field, Blackman & Keto (2011) imagine the ISM as a turbulent cascade of mass and energy from larger to smaller scales. The transfer takes place through fragmentation of larger scale clouds which is motivated by the decay of the turbulence. In this picture the gravitational and kinetic energies of the clouds in the ISM are in virial equilibrium with an external pressure. The concept of a maximum mass for stable equilibrium applies to these clouds in virial equilibrium the same way as it does to the BES in hydrostatic equilibrium. As with the BES, the larger scale clouds continuously lose their internal kinetic energy through dissipation of their turbulence. Unlike the BES, these larger clouds whose dynamics are dominated by the inertial forces of the supersonic turbulence can fragment into smaller clouds whose masses are below their maximum stable masses, at least for the moment until they too lose energy through turbulent dissipation. This process continues to smaller and smaller scales until the clouds are small enough to be supported by subsonic turbulence and thermal pressure. This is the sonic scale and the scale of the starless cores.

This process imagines that cores with subsonic turbulence are created in a range of masses above and below the maximum stable mass. Those cores with higher masses immediately begin contraction to star formation. These are short-lived and rarely observed. We are left with cores whose masses can be supported by a combination of thermal and subsonic turbulent energy. These are the cores we see in the Taurus star forming region evolving to star formation through the decay of their subsonic turbulence. Other cores whose masses are small enough to be supported by thermal energy alone may never form stars. Many of the cores in the Pipe nebula are in this category (Lada et al. 2008).

8 DISCUSSION

The conclusion of our research on L1544 is that this core is contracting in a way that is very specifically matched by the contraction of a QE-BES. The comparison with the NE-BES indicates that even a 10% deviation from (unstable) equilibrium will create contraction velocities incompatible with the observations. Other modes of contraction with supersonic velocities either at large or small scales, for example, but not limited to, the LP flow or the SIS inside-out collapse, are also precluded by the data. In this sense, the LP and SIS models serve as examples to stand for many other types of models with supersonic flows. For example, the LP model with its supersonic velocities at the cloud boundary may be representative of other models that form the starless cores by compression of larger-scale flows or models of cores that accrete gas from larger scales. The NE-BES model may be representative of many types of models characterized by free-fall collapse. The SIS model may be representative of many types of models that lack pressure support at the center, for example accretion onto a gravitational point source or a pressure-free sink cell. In this sense, although the several models considered in this study are quite specific, they suggest against many other types of models for the starless cores particularly those with supersonic velocities either at small or large scales.

Stressing the conditionals here, if it is hard to imagine that L1544 can so closely resemble a quasi-equlibrium hydrostatic cloud without actually being one, and if it is hard to imagine conditions in the turbulent ISM that can create hydrostatic cores, then our conclusion of the quasi-hydrostatic state of L1544 goes head-to-head against the strong conclusion from some of the numerical hydrodynamical simulations that hydrostatic clouds cannot be created in the turbulent ISM.

However, we have so far studied only this one core at this level of detail, and the observation of the water emission line in L1544 is unique among starless cores. While L1544 shows no indication that it is unique among the cores in Taurus, definitive conclusions obviously should not be drawn from this one example. Further observations of other cores are needed. Because the Herschel Space Observatory is no longer operating, we will have to find other tracers that isolate the conditions in the core centers. The deuterated species of some molecules are possibilities (van der Tak, Caselli & Ceccarelli 2005; Caselli et al. 2003).

P. Caselli acknowledges the financial support of the European Research Council (ERC; project PALs 320620)

REFERENCES

Aguti E. D., Lada C. J., Bergin E. A., Alves J. F., Birkinshaw M., 2007, ApJ, 665, 457
Alves J. F., Lada C. J., Lada E. A., 2001, Nature, 409, 159
Ballesteros-Paredes J., Klessen R. S., Vázquez-Semadeni E., 2003, ApJ, 592, 188
Beichman C. A., Myers P. C., Emerson J. P., Harris S., Mathieu R., Benson P. J., Jennings R. E., 1986, ApJ, 307, 337
Broderick A. E., Keto E., 2010, ApJ, 721, 493
Broderick A. E., Keto E., Lada C. J., Narayan R., 2007, ApJ, 671, 1832
Broderick A. E., Narayan R., Keto E., Lada C. J., 2008, ApJ, 682, 1095

Caselli P. et al., 2012, ApJ Lett, 759, L37
Caselli P. et al., 2010, A&A, 521, L29
Caselli P., van der Tak F. F. S., Ceccarelli C., Bacmann A., 2003, A&A, 403, L37
Caselli P., Walmsley C. M., Tafalla M., Dore L., Myers P. C., 1999, ApJ Lett, 523, L165
Caselli P., Walmsley C. M., Zucconi A., Tafalla M., Dore L., Myers P. C., 2002, ApJ, 565, 344
Ciolek G. E., Basu S., 2000, ApJ, 529, 925
Crapsi A., Caselli P., Walmsley M. C., Tafalla M., 2007, A&A, 470, 221
Dubernet M.-L., Daniel F., Grosjean A., Lin C. Y., 2009, A&A, 497, 911
Evans, II N. J., Rawlings J. M. C., Shirley Y. L., Mundy L. G., 2001, ApJ, 557, 193
Field G. B., Blackman E. G., Keto E. R., 2011, MNRAS, 416, 710
Foster P. N., Chevalier R. A., 1993, ApJ, 416, 303
Goodman A. A., Barranco J. A., Wilner D. J., Heyer M. H., 1998, ApJ, 504, 223
Keto E., Broderick A., Lada C. J., Narayan R., 2006, ArXiv Astrophysics e-prints
Keto E., Caselli P., 2008, ApJ, 683, 238
Keto E., Caselli P., 2010, MNRAS, 402, 1625
Keto E., Field G., 2005, ApJ, 635, 1151
Keto E., Rawlings J., Caselli P., 2014, MNRAS, 440, 2616
Keto E., Rybicki G., 2010, ApJ, 716, 1315
Keto E. R., 1990, ApJ, 355, 190
Klessen R. S., Ballesteros-Paredes J., Vázquez-Semadeni E., Durán-Rojas C., 2005, ApJ, 620, 786
Lada C. J., Bergin E. A., Alves J. F., Huard T. L., 2003, ApJ, 586, 286
Lada C. J., Muench A. A., Rathborne J., Alves J. F., Lombardi M., 2008, ApJ, 672, 410
Larson R. B., 1969, MNRAS, 145, 271
Larson R. B., 1981, MNRAS, 194, 809
Lee C. W., Myers P. C., Tafalla M., 2001, ApJ Suppl, 136, 703
Leung C. M., Kutner M. L., Mead K. N., 1982, ApJ, 262, 583
Li Z.-Y., 1999, ApJ, 526, 806
Mac Low M.-M., Klessen R. S., 2004, Reviews of Modern Physics, 76, 125
Mouschovias T., 2001, in Astronomical Society of the Pacific Conference Series, Vol. 248, Magnetic Fields Across the Hertzsprung-Russell Diagram, Mathys G., Solanki S. K., Wickramasinghe D. T., eds., p. 515
Myers P. C., 1983, ApJ, 270, 105
Myers P. C., Benson P. J., 1983, ApJ, 266, 309
Myers P. C., Evans, II N. J., Ohashi N., 2000, Protostars and Planets IV, 217
Myers P. C., Goodman A. A., 1988, ApJ Lett, 326, L27
Nakano T., 1998, ApJ, 494, 587
Nielbock M. et al., 2012, A&A, 547, A11
Offner S. S. R., Krumholz M. R., Klein R. I., McKee C. F., 2008, AJ, 136, 404
Ogino S., Tomisaka K., Nakamura F., 1999, PASJ, 51, 637
Penston M. V., 1969, MNRAS, 144, 425
Pineda J. E., Goodman A. A., Arce H. G., Caselli P., Foster J. B., Myers P. C., Rosolowsky E. W., 2010, ApJ Lett, 712, L116
Redman M. P., Keto E., Rawlings J. M. C., 2006, MNRAS, 370, L1
Shu F. H., 1977, ApJ, 214, 488
Shu F. H., Adams F. C., Lizano S., 1987, ARAA, 25, 23
Tachihara K., Onishi T., Mizuno A., Fukui Y., 2002, A&A, 385, 909
Tafalla M., Mardones D., Myers P. C., Caselli P., Bachiller R., Benson P. J., 1998, ApJ, 504, 900
Tafalla M., Myers P. C., Caselli P., Walmsley C. M., Comito C., 2002, ApJ, 569, 815
van der Tak F., Caselli P., Ceccarelli C., 2005, in ESA Special Publication, Vol. 577, ESA Special Publication, Wilson A., ed., pp. 429–430
van Dishoeck E. F., Blake G. A., 1998, ARAA, 36, 317
Ward-Thompson D., Motte F., Andre P., 1999, MNRAS, 305, 143
Whitworth A. P., Bhattal A. S., Francis N., Watkins S. J., 1996, MNRAS, 283, 1061
Wilson T. L., Rood R., 1994, ARAA, 32, 191